2025-32-0056/20259256 Published 03 Nov 2025

Validation of an Integrated Ignition-Combustion Model for Premixed Hydrogen-Air Flames under Lean Conditions

Marco Pretto University of Udine

Fabio Bozza University of Naples "Federico II"

Pietro Giannattasio University of Udine

Vincenzo De Bellis and Emanuele Ugliano University of Naples "Federico II"

Citation: Pretto, M., Bozza, F., Giannattasio, P., De Bellis, V. et al., "Validation of an Integrated Ignition-Combustion Model for Premixed Hydrogen-Air Flames under Lean Conditions," SAE Technical Paper 2025-32-0056, 2025, doi:10.4271/2025-32-0056.

Received: 16 May 2025 Revised: 11 Jul 2025 Accepted: 14 Jul 2025

Abstract

Recent climate changes, driven by greenhouse gas emissions, along with global regulations aimed at mitigating these effects, have intensified research on carbon-free fuels. Among these, hydrogen stands out as one of the most promising options. In this study, use is made of a recent 1D kernel expansion model developed by the authors, which is based on the conservation equations of mass, energy and deficient reactant. The theory of transient thermo-diffusion is also adopted to estimate the reactant and temperature gradients at the outer flame surface. The kernel expansion model accounts for the variability of thermodynamic properties both inside and outside the flame volume, including high-temperature ionization and dissociation effects. The kernel expansion model is used until the non-linear stretch effects are sufficiently relaxed. Subsequently, the propagation of the premixed flame is described by means of a two-zone combustion model. During both phases, the effects of hydrodynamic and thermo-diffusive instabilities are accounted for. The former are modeled considering the flame wrinkling produced by the density discontinuity across the flame, evolving towards a self-similar fractal-like behavior. The latter, induced by a less-than-unity Lewis number, are modeled introducing an equivalent flame consumption speed to quantify the increase in flame expansion velocity. The model is validated against experimental data from literature obtained for premixed hydrogen-air flames propagating in an optically accessible spherical bomb. The data used for model validation refer to quiescent conditions at multiple lean equivalence ratios (from 0.45 to 0.97). The capabilities of the present model are assessed with reference to the measured time histories of chamber pressure, flame radius and expansion speed. A good agreement is achieved across all the test cases considered, confirming the consistency of the integrated ignition-combustion model proposed in this work.

Introduction

In the past 15 years, the need to decarbonize the mobility and the power energy sectors has been the main reason for worldwide research and development on alternative low- or zero-carbon fuels, such as hydrogen. It is a common feeling, especially in Europe, that the transition to a decarbonized economy will require hydrogen on a large scale, and in particular clean hydrogen produced by renewable energy sources [1].

Clean hydrogen can in fact play a key role for long-term energy storage and for reducing greenhouse gas emissions, especially in sectors where electrification is much more difficult, such as heavy-duty long-distance transport, and energy-intensive industry. As an example, hydrogen-powered internal combustion engines (H2-ICEs) are foreseen as a promising alternative to conventional fossil-fueled propulsion systems, given their potential to curb CO_2 and NO_x emissions. To this aim, however, H2-ICEs must operate under a homogenous lean or ultra-lean fuel/air mixture, simultaneously exploiting the well-known wide flammability range of hydrogen and its high flame propagation speed. Both heavy-duty and light-duty applications are under development, with thermal efficiencies as high as 42-45% [2,3].

In addition to the direct conversion of hydrogen in fuel cell systems, its use in existing thermal devices and combustion systems brings new challenges to the already complex problem of combustion modeling. Like any gaseous mixture, burning hydrogen/air mixtures undergo a strong thermal expansion, which may lead to the so-called hydrodynamic flame instability. The latter, commonly referred to as Darrieus-Landau (DL) instability, was first identified by Darrieus (1938) and later formalized by Landau (1944) [4,5]. Their seminal work revealed that the density discontinuity $\Theta = \rho_u/\rho_b$ caused by thermal expansion during combustion can induce perturbations in premixed flames, leading to an increase in effective flame area and combustion speed [6,7]. In general, any small perturbation bending an infinitely thin flame front continuously grows at a rate that depends on the thermal expansion ratio, and as such it is an intrinsic characteristic of any gaseous premixed flame [8]. As soon as the flame radius is greater than a critical value, ligaments start appearing on the flame surface, grow over time, and produce a typical cellular structure of the surface. Pelce and Clavin [9] showed that the typical length scale of the cellular structures exceeds the flame thickness by two orders of magnitude (large-scale cellularity). The time-dependent stretch of a spherically expanding flame induces a continuous increase in the amplitude of the perturbations over time, evolving towards a fractal flame structure with a cascade of front cells of different sizes superposed on each other [10].

In addition, lean or ultra-lean hydrogen/air burning mixtures exhibit larger species diffusivities compared to the molecular heat diffusivity (Lewis number, $Le < 1$), producing the so-called Thermo-Diffusive (TD) instabilities, also called Lewis number effects. TD instability results from the competition between thermal and mass diffusion processes within the flame. When the thermal diffusivity of the limiting reactant exceeds its mass diffusivity (i.e., $Le > 1$), the flame temperature tends to decrease, suppressing flame perturbations and thereby stabilizing the flame [11]. Conversely, if the thermal diffusivity is lower, or the limiting reactant exhibits relatively high molecular diffusivity ($Le < 1$), preferential diffusion enhances the delivery of the reactant to the reaction zone, leading to an increase in the consumption speed due to a higher local temperature gradient. Theoretical analyses based on a detailed chemistry simulation of a 2D expanding, thermo-diffusively unstable hydrogen flame, have shown that this phenomenon becomes even more relevant with increasing pressures [12, 13, 14]. Similarly to the DL instability, TD effects produce small-scale cells or finger-like large-scale cells that begin to appear when the flame radius is greater than a second critical radius, usually smaller than the DL one.

In essence, DL and TD effects can coexist, and both determine the formation of a highly stretched wrinkled structure (cellular stretching), which, moreover, interacts with the additional stretch possibly induced by an underlying turbulent flow field (turbulent stretching) [15]. Additionally, this wrinkled flame can form only if the flame kernel has ignited successfully, which depends on the mixture properties as well as on the ignition strategy, sometimes leading to widely different kernel formation times upon marginal alterations of even a single parameter [16]. Therefore, proper simulation of hydrogen/air flames implies being able to model multiple flame regimes from the spark plug to the wall of the combustion chamber.

In this paper, an attempt is made to describe in a 1D/0D modeling framework the complete evolution of a burning hydrogen-air mixture within a spherical combustion bomb. The combustion chamber is modeled as a spherical volume with a two-zone approach, and the simulation is split into two phases. During the first phase a 1D kernel expansion model is applied, which is based on the conservation equations of mass, energy, and deficient reactant. The reactant conservation is often neglected in the literature following Herweg and Maly's seminal model for spark-ignited ICEs [17], but Ko et al.'s approach [18] showed that this conservation must be included when the kernel radius is just a few millimeters. These equations are supported by the theory of transient thermo-diffusion, which is employed to estimate the reactant and temperature gradients at the outer flame surface [19,20]. In this phase, the kernel expansion is strongly affected by the imbalance between species and thermal diffusion, which leads to non-linear flame stretch, and by the ignition strategy [21]. Finally, when the flame kernel grows large enough to make stretch-related effects practically irrelevant, the simulation switches to a more conventional 0D two-zone approach. At this stage, the flame is assumed to propagate in a laminar regime, and the negligible flame stretch enables dropping the reactant conservation equation. During the entire flame expansion, the previously described DL and TD instabilities are considered. On the modeling of DL instability, Zaytsev [22] and Chaudhuri [23] tackle this topic considering 2D and 3D tubes, respectively, and a planar flame configuration, whereas Bychkov [24] considers a convex flame front. According to these studies, the initial rise in flame speed is related to the density ratio between burned and unburned gases, but beyond a critical radius the further increase in flame speed depends also on the kernel size. Regarding the modeling of TD instability effects, both Berger [25] and Howarth [26,27] have proposed practical approaches to quantify the resulting flame speed increase. Berger's correlation depends on density ratio, effective Lewis number, and Zel'dovich number, whereas Howarth's correlation relies on parameter ω_2, which represents the growth rate of TD perturbations and depends on effective Lewis, Prandtl, and Zel'dovich numbers. However, in the authors' knowledge no approach exists that combines the onset and development of both DL and TD instabilities with the processes associated with the flame kernel growth after a spark ignition. Aiming to investigate the effects of DL and TD instabilities on the flame expansion, the present study focuses exclusively on hydrogen combustion in quiescent conditions. Accordingly, the influence of turbulence fields and their interaction with both early kernel growth and flame instabilities is left to future developments.

The paper is organized as follows: firstly, the methodology employed to describe the initial kernel growth and the subsequent two-zone approach are presented. Then, a detailed description of the way the DL and TD

instabilities are included in the model is provided. Finally, the model is applied to replicate experimental data taken from Goulier et al. [28,29]. Comparisons will be presented and discussed with reference to the measured time histories of chamber pressure, flame radius and expansion speed. Although the literature data [28,29] refer to both quiescent and turbulent flow conditions, in this work the model is applied only to the laminar cases at multiple lean equivalence ratios (from 0.45 to 0.97). As previously noted, this represents a fundamental prerequisite for subsequent extension to turbulent cases.

Methodology

Kernel Expansion Model

The 1D kernel expansion model used in this work has been formulated recently by the present authors [19], and its main steps are recalled in this subsection. The model is split into an initiation stage, prompted by the electrical breakdown between the electrodes, and a proper 1D early expansion stage, controlled by the interaction between diffusive, reactive, and convective processes.

The kernel initiation is modeled as the result of the shock wave expansion caused by the local overpressure that results from supplying breakdown energy E_{bd} to the spark plug. The breakdown activates a cylindrical plasma volume ($V_i = \pi r_{i,cyl}^2 d_g$) after a relaxation time t_i necessary to bring the local pressure within 10% of chamber pressure p. Within this time, E_{bd} also raises the enthalpy from h_u, value of the unburned mixture, to h_i, value of the hot plasma, changing also the local density from ρ_u to ρ_i. Following the comprehensive analysis made by Meyer and Wimmer [30], the relevant end-of-breakdown conditions are determined according to the three equations below, which derive from numerical solutions of mass, momentum, and energy conservation equations written in cylindrical coordinates and applied to the spark-gap column affected by E_{bd}. The third equation also enables estimating temperature T_i, being $h_i = h_i(T_i)$, with typical values of it ranging between 4000 K and 7000 K depending on mixture type and energy deposition efficiency η_{bd}.

$$r_{i,cyl} = 0.5 r_c = 0.5\left[E_{bd} / \left(3.94 \pi p d_g\right)\right]^{\frac{1}{2}}, \tag{1a}$$

$$t_i = 1.5 t_c = 1.5\left(r_c / \sqrt{p\gamma_u / \rho_u}\right), \tag{1b}$$

$$\left(h_i - h_u\right)\rho_i V_i = \eta_{bd} E_{bd}. \tag{1c}$$

Finally, for consistency with the expansion of a spherical flame, the activated volume is converted to a sphere using $r_i = \sqrt[3]{3V_i / 4\pi}$.

Upon determination of the initial conditions, the expansion model for the early growth of the flame kernel is applied. This model is based on multiple assumptions duly discussed in reference [19]. Key aspects are the constant pressure and the description of the combustion by a one-step reaction with activation temperature T_a, controlled by the deficient reactant, e.g. the fuel in a lean mixture. The model is based on the conservation equations of kernel energy and mass fraction Y_A of the limiting reactant at the outer flame surface, and on relevant outcomes of the transient thermo-diffusion theory. In particular, the model considers the time-dependent radial profiles of temperature, $T(r,t)$, and deficient reactant mass fraction, $Y_A(r,t)$, in the pre-heat and reactant depletion zones outside the flame. These profiles allow to estimate the gradients $\partial T/\partial r$ and $\partial Y_A/\partial r$ at flame radius $r_f(t)$ during the kernel expansion, occurring at speed $v_f = dr_f/dt$. For an expanding spherical kernel having mass $m_f(t)$ and uniform temperature $T_f(t)$, the conservation equations of energy and mass fraction Y_A are written in the following form [19]:

$$m_f c_{p,f} \frac{dT_f}{dt} = \left(\rho_u A_f S_L^0 \omega_f + \dot{m}_{en}\right) Q_f + k_{u,f} A_f C_T \left.\frac{\partial T}{\partial r}\right|_{r_f} + P_e, \tag{2}$$

$$\frac{1}{Le}\left(\frac{k}{c_p}\right)_{u,f} C_A \left.\frac{\partial Y_A}{\partial r}\right|_{r_f} = Y_{Au}\rho_u S_L^0 \omega_f, \tag{3}$$

where quantities related to the fresh mixture at T_f are identified with $[\cdot]_{u,f} = [\cdot]_u(T_f)$, while those concerning the burned gases as $[\cdot]_f$. In equations (2) and (3), $Q_f = h_{u,f} - h_f$ is the heat of combustion, h is the absolute specific enthalpy, k and c_p are the thermal conductivity and specific heat at constant pressure, respectively, Le is the Lewis number, P_e is the effective glow-phase electric power, and $\dot{m}_{en}$ is the ignition-affected entrainment mass flow rate. Finally, ω_f expresses the dependency on the reaction rate on T_f through T_a as follows:

$$\omega_f = \left(\frac{T_f}{T_{ad}}\right)^2 \exp\left(-\frac{T_a}{2}\left(\frac{1}{T_f} - \frac{1}{T_{ad}}\right)\right). \tag{4}$$

To close the two-equation system (2,3) the gradients of temperature and deficient reactant at r_f must be determined. This is done using the results of transient thermo-diffusion [31], which provides the following expressions for these two gradients:

$$\left.\frac{\partial T}{\partial r}\right|_{r_f} = -\frac{f_{uT}}{R}\left[\theta_f + \theta_i\left(\vartheta\left(\exp\left(x_1\right)\right) - 1\right)\right]\frac{\left(T_{ad} - T_u\right)}{l_T^0}, \tag{5}$$

$$\left.\frac{\partial Y_A}{\partial r}\right|_{r_f} = \frac{f_{uY}}{R}\vartheta\left(\exp\left(x_2\right)\right)\frac{Y_{Au}}{l_T^0}, \tag{6}$$

where $x_1 = -\pi^2 f_{uT}^2 \tau / R^2$ and $x_2 = -\pi^2 f_{uY}^2 \tau / LeR^2$. These expressions rely on several non-dimensional terms, reported below and defined with respect to the values

of the planar adiabatic laminar flame, in particular to its temperature T_{ad} and absolute speed $v_L^0 = \left(\rho_u / \rho_{ad}\right) S_L^0$:

$$l_T^0 = \frac{k_{ad} / c_{p,ad}}{\rho_{ad} v_L^0},\ \theta = \frac{T - T_u}{T_{ad} - T_u},\ \tau = t\frac{v_L^0}{l_T^0},\ R = \frac{r_f}{l_T^0}, \tag{7}$$

Expressions in (5, 6) are completed by defining normalized flame speed $U = v_f / v_L^0$, Jacobi theta function $\theta\left(x\right) = 1 + \sum_{n=1}^{+\infty} x^{n^2}$, and f_{uT}, f_{uY} as follows:

$$f_{uT} = \left[\int_1^{+\infty} \frac{1}{s^2} \exp\left(-\frac{RU}{2}\left(s^2 - 1\right)\right) ds\right]^{-1}, \tag{8a}$$

$$f_{uY} = \left[\int_1^{+\infty} \frac{1}{s^2} \exp\left(-\frac{LeRU}{2}\left(s^2 - 1\right)\right) ds\right]^{-1}. \tag{8b}$$

Finally, coefficients C_A and C_T are introduced in equations (2) and (3) to account for the variation of thermodynamic properties during the expansion. Their terminal values, that ensure consistency with the adiabatic planar flame (U = 1) and the stationary flame ball (U = 0), are reported in Table 1. They were assumed to take on intermediate values for different expansion velocities upon calibration using literature data, as detailed by the authors in their work [19].

The numerical solution of the two-equation system (2,3) over each time step enables the computation of the (T_f, v_f) pair at the new time, from which the new r_f and ultimately the new kernel mass m_f can be calculated.

The summarized early kernel expansion model is applied to reconstruct the fast energy-driven expansion right after the ignition, as well as the kernel growth affected by non-linear stretch that immediately follows. However, the use of hydrogen is associated with flame instabilities that, breaking the smoothness of the flame surface, can accelerate the growth already during the early kernel development. This acceleration is estimated by keeping the same 1D formulation but introducing instability-related coefficients x_{DL} and x_{TD} as multipliers to $S_L^0 \omega_f$. All details on these two coefficients and their estimation are reported in the following subsections.

TABLE 1 Values of C_A and C_T for adiabatic planar flame and flame ball.

	Adiabatic planar, U = 1	Flame ball, U = 0
C_A	$\frac{\left(k / c_p\right)_{ad}}{\left(k / c_p\right)_{u,ad}}$	1
C_T	$\frac{\left(h_{u,ad} - h_{ad}\right) k_{ad}}{c_{p,ad}\left(T_{ad} - T_u\right) k_{u,ad}}$	$\frac{h_{u,z} - h_z}{c_{p,u,z}\left(T_{ad} - T_u\right)}$

Two-Zone Combustion Model

A simpler 0D two-zone combustion model is activated once the non-linear stretch effects are sufficiently relaxed. This is because when the flame kernel has grown large enough, heat of combustion and thermal losses toward the unburned gases are sufficiently balanced. As a consequence, the kernel temperature becomes almost constant before the compression effects start being relevant, and the flame stretch plays a minimal role in influencing the expansion. The switch to the two-zone model is carried out when the aforementioned correction ω_f drops to a value close to unity (in practice, when ω_f < 1.1, which means that $T_b = T_f \cong T_{ad}$) In this second phase, the combustion bomb is still divided into a burned zone and an unburned zone separated by an infinitely thin flame front, while the flame expansion can be simulated using just the mass and energy conservation equations for both zones. The energy conservation equations below are solved to derive the instantaneous temperature of each zone:

$$\frac{dm_u e_u}{dt} = \frac{dm_u}{dt} h_u - \frac{dQ_{wu}}{dt} - p\frac{dV_u}{dt}, \tag{9}$$

$$\frac{dm_b e_b}{dt} = \frac{dm_b}{dt} h_u - \frac{dQ_{wb}}{dt} - p\frac{dV_b}{dt}. \tag{10}$$

In the present case, being the flame centrally ignited and always far away from the walls, the heat transfer terms can be considered negligible $\left(\frac{dQ_{wu}}{dt} = \frac{dQ_{wb}}{dt} = 0\right)$, and, considering the pressure inside the bomb uniform, the ideal gas law can be used to close the problem. Regarding the mass conservation, the burning rate is calculated as:

$$\frac{dm_b}{dt} = -\frac{dm_u}{dt} = \rho_u A_L S_L x_{DL} x_{TD}. \tag{11}$$

Here, ρ_u denotes the density of the unburned gas, m_b is the burned mass, A_L refers to the spherical surface area of the laminar front and S_L denotes the unburned-relative laminar flame speed, which includes the aforementioned very reduced ω_f correction ($S_L = S_L^0 \omega_f$). The burned-relative expansion speed would hence be:

$$S_b = \frac{\rho_u}{\rho_b} S_L. \tag{12}$$

The unburned and burned thermodynamic properties were estimated using the CEA code [32], while S_L^0 was calculated using a 1D planar flame simulation based on Cantera software package and adopting the kinetic mechanism proposed by Zhang [33]. Finally, terms x_{DL} and x_{TD} in eq. (11) account for the flame speed increase due to the effects of hydrodynamic and thermo-diffusive instabilities, respectively, as detailed in the subsequent sections.

Once all the terms appearing in eqs. (9) to (11) have been determined, the flame expansion speed v_f can be calculated for each time step. However, while in the kernel expansion model v_f is the direct solution of eqs. (2, 3), in the two-zone approach it arises from the solution of mass and energy equations in the burned zone as follows:

$$v_f = \frac{dr_f}{dt} = \frac{r_f}{3}\frac{\dot{V}_b}{V_b} = \frac{r_f}{3}\left(\frac{\dot{m}_b}{m_b} + \frac{\dot{T}_b}{T_b} - \frac{\dot{p}}{p}\right). \tag{13}$$

Modeling of Hydrodynamic Instability

As already mentioned, hydrodynamic instabilities start raising the flame expansion speed after a critical threshold size has been reached. For hydrogen flames, the critical radius r_{cDL}, expressed in meters, after which the DL instabilities start to occur, is calculated according to the correlation proposed in [34]:

$$r_{c_{DL}} = 0.0125 \cdot 1.5225\left(\frac{T_u}{373}\right)^{0.8769}\left(\frac{p}{2.5}\right)^{-1.2990}\varphi^{1.2384}, \tag{14}$$

where T_u, p, and φ are, respectively, the unburned gas temperature, expressed in Kelvin, the pressure, expressed in bar, and the mixture equivalence ratio. Above the critical radius, the flame speed increase related to the hydrodynamic instabilities is computed as:

$$x_{DL} = \frac{S_{DL}}{S_L} = 1 + p_g \frac{\left[4\Theta\left(\Theta - 1\right)^2\right]}{\left[\Theta^3 + \Theta^2 + 3\Theta - 1\right]}, \tag{15}$$

Θ being the density ratio. Eq. (15) has been derived in literature [24] for steady flames propagating in a 2D tube, where the geometrical parameter p_g = 0.5, and in a 3D cylinder, where p_g = 1. In the present case, which refers to an unsteady spherically and free expanding flame, parameter p_g can be viewed as a tuning constant, and it is set to 0.6 in the present work. Eq. (15) is adopted until the flame radius exceeds the r_{cDL0} threshold ($r_{cDL0} \cong 4\, r_{c_{DL}}$). During this time, the initial flame ligaments present on the flame surface produce additional inner cells and the flame surface exhibits a fractal-like cellularity evolution. Beyond threshold r_{cDL0}, the flame speed enhancement due to hydrodynamic instabilities is given by the following equation:

$$x_{DL} = x_{DL0}\left(\frac{r_f}{r_{cDL0}}\right)^D, \tag{16}$$

where x_{DL0} is the enhancement value at r_{cDL0}, and D is the fractal excess, evaluated according to Bychkov [24] as:

$$D = \frac{\log\left(x_{DL0}\right)}{\log\left(\frac{r_{c_{DL0}}}{r_{c_{DL}}}\right)}. \tag{17}$$

Modeling of Thermo-Diffusive Instability

The second type of flame instability is caused by thermo-diffusive (TD) effects associated primarily with low Lewis numbers, which are typical of lean hydrogen/air mixtures. The TD effects begin to appear when the flame radius is greater than another critical radius, denoted as r_{cTD}, defined by Beeckmann [34] as:

$$r_{c_{TD}} = 0.0125 \cdot 0.9137\left(\frac{T_u}{373}\right)^{0.8146}\left(\frac{p}{2.5}\right)^{-1.2366}\varphi^{1.2728}. \tag{18}$$

Beyond this threshold, according to Howarth et al.'s correlation [26,27] the TD-related effective propagation speed ratio is:

$$\frac{S_{TD}}{S_L} = \begin{cases} \exp\left(0.08\omega_2\right) & \text{if } \dfrac{p}{1.013} < \Pi_c \\ \left(1 + 0.47\omega_2\right) & \text{if } \dfrac{p}{1.013} > \Pi_c \end{cases} \tag{19a) (19b}$$

$$\Pi_c = \left(\frac{20\varphi}{7 - 2\theta_{TD}}\right)^{\frac{150}{21 + 10\,\theta_{TD}}} \tag{20}$$

$$\theta_{TD} = \frac{T_u}{300} \tag{21}$$

In these expressions, parameter ω_2 represents the growth rate of the TD perturbations, and depends on Lewis, Prandtl and Zel'dovich numbers. Above a certain critical Lewis number (around 0.6), parameter ω_2 assumes negative values, meaning that TD instabilities no longer occur. The critical pressure, Π_c, indicates a threshold level separating two regimes with distinct dynamic characteristics of the TD instabilities.

The TD-related flame speed enhancement is then calculated as:

$$x_{TD} = 1 + c_{TD}\left(\frac{S_{TD}}{S_L} - 1\right), \tag{21}$$

c_{TD} being a model constant correcting the overall TD impact on the flame speed when the thermodynamic conditions differ from the ones considered by Howarth [26,27]. As an example, Meziat et al. [15] showed that the above correlations, although working very well, slightly overestimate the expansion speed. Consistently with these authors' findings, in the present work c_{TD} is set to 0.9.

The instability correlations defined above provide the "fully developed" flame speed enhancement factors x_{LD} and x_{TD}, but their terminal values are reached only after the kernel has grown sufficiently large, while their intensity changes over the entire expansion process. Their evolution over time will be presented in the results discussion section.

Model Setup

The reliability of the integrated ignition-combustion model developed in this work is validated against the experimental data presented by Goulier et al. [28,29]. These authors tested different hydrogen-air mixtures with hydrogen volume fractions of 16%, 20%, 24%, and 28% in a 563 mm inner diameter combustion bomb. For all test points, the initial pressure and temperature were set to 1.01 bar and 293 K, respectively. The experiments were carried out at different turbulence levels in the combustion chamber, but the present work, as already stated, only considers the tests under quiescent conditions.

As shown in the previous section, the present integrated model requires the assignment of some input parameters, classifiable into two groups. The first group includes thermochemical data, which depend on fuel type, temperature, pressure, and mixture properties (such as equivalence ratio and inert gas content). These data are evaluated by means of software package Cantera using Zhang et al.'s reaction mechanism [33], and include the planar adiabatic laminar flame speed, the mixture Lewis number, and the equivalent activation energy, evaluated according to the procedure reported in literature [7,35]. The values of these parameters, computed for the initial conditions and reported in Table 2, are quite similar to the ones given by Goulier [28,29]. These parameters are updated during the simulation according to the increasing chamber pressure and temperature in the unburned zone.

The second group of model parameters refers to the characteristics of the spark-ignition system, such as

- spark plug gap (d_g = 0.6 mm),
- breakdown energy supplied to the kernel (E_{bd} = 0.3 mJ),
- breakdown efficiency (η_{bd} = 1),
- electrical energy supplied via arc/glow (E_e = 6 mJ),
- arc/glow duration (t_e = 0.3 ms),
- electrode gap efficiency (η_{gap} = 1),
- area used to evaluate the entrainment of fresh charge between the electrodes during the spark (C_d = 0.02 mm^2).

Since these spark-ignition characteristics were not specified by Goulier [28,29], the authors adopted the values reported in brackets, which refer to a standard ignition system for automotive applications, while retaining the sub-models employed in their previous work [19] and derived from Ko et al.'s contribution [18]. Their application yielded the $P_e(t)$ to be used in the kernel energy conservation of equation (2), which, integrated over t_e, resulted in an effective arc/glow deposition efficiency of around 37%. This value agrees well with Herweg and Maly's estimate for a capacitive discharge in a near-quiescent volume [17], and implies that the remaining 63% of E_e is lost via heat transfer to the electrodes. Note that for lean hydrogen knowledge of the exact ignition parameters is not critical because of the low Lewis number, which ensures successful ignition with minimal energy and influences only moderately the following early expansion. This is already visible for methane/air mixtures, which have $Le \cong 1$ [21].

Sensitivity Analysis of the Integrated Model

In the previous sections several input variables have been defined for the integrated ignition-combustion model proposed in this work, which include the input data of the kernel model, as well as the tuning parameters chosen for the DL and TD instabilities. Therefore, in this section a sensitivity analysis is conducted to examine the impact of these parameters on the behavior of the proposed model.

Kernel Expansion Model Input Data

The first analysis is conducted on the kernel expansion for a representative case, chosen as that with 28% hydrogen volume fraction. Figure 1 illustrates the relative time variation required to reach flame radii values of 2 mm, taken as the marker of a successful ignition, and 36.26 mm, which corresponds to r_{cDL} for this case, resulting from a ± 20% change in the kernel expansion model parameters. The relative time variations in Figure 1 were computed by averaging the time differences resulting from separate application of the two variations (+20% and -20%) with respect to the reference time (no parameter change) and normalizing the outputs against the latter. Figure 1 highlights that the effects of these variations are already modest at 2 mm (a few percentage points), whereas at 36.26 mm their effect is minimal (below 0.3% in all cases). The numerical findings for the smaller radius underline that the parameters controlling the arc/glow phase, E_e and t_e, have the greatest influence,

TABLE 2 Thermochemical properties for mixtures with different hydrogen volume fractions.

Initial Press. (bar)	Initial Temp. (K)	H_2 vol. fract. (%)	φ	S_L^0 (m/s)	Lewis Number	Activation Energy (kJ/mol)
1.01	293	16	0.453	0.440	0.512	171.1
		20	0.596	0.910	0.541	156.3
		24	0.752	1.390	0.761	152.4
		28	0.926	1.910	0.994	159.2

FIGURE 1 Relative time variation to reach a kernel radius of 2 mm (blue bars, left axis) and r_{cDL} = 36.26 mm (red bars, right axis) resulting from a ± 20% change in the kernel model parameters for 28% H_2 concentration (φ = 0.926).

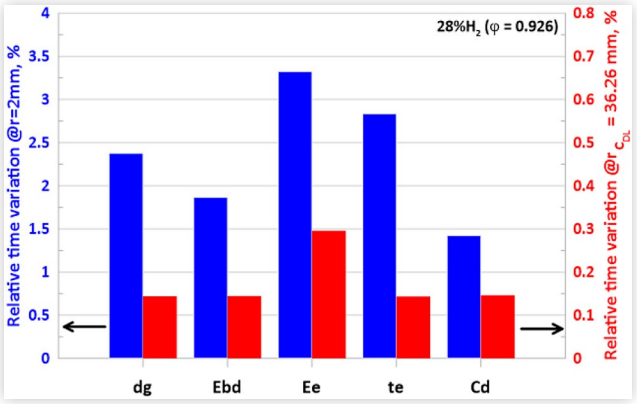

followed by electrode gap d_g, all of which are associated with time variations in excess of 2%. However, the minor time variations reported for r_{cDL} suggest that the influence of these parameters on the overall combustion is negligible.

To further emphasize the limited impact of the kernel parameters, the two with greatest influence, d_g and E_e, were conjointly raised and lowered by 50% for both the leanest (16% H_2) and richest (28% H_2) cases considered in this work. This computation led to the plots in Figure 2, which report flame expansion speed and chamber pressure over time for the three sub-cases (reference, +50%, and -50%) included for both mixtures. Apart from minor flame speed differences for the 28% hydrogen case towards the end of the electricity-supported expansion, any other variations from the reference values are negligible for both flame speed and pressure time histories. This confirms that the key element is the use of a well-founded kernel expansion model, whereas the ignition parameters have limited impact on the results as long as reasonable values are chosen. Instead, it is much more important to detect correctly the effects of different hydrogen concentrations through the mixture and flame parameters (e.g. S_L^0, *Le*), which control both the early kernel growth and the subsequent flame expansion.

Flame Instability Tuning Constants

The second analysis targets the tuning variables for the DL and TD instabilities, which are p_g and c_{TD} respectively. For this study the case with 16% hydrogen volume fraction is selected, as it exhibits both instabilities at reasonably low flame radii. The analysis is conducted by examining pressure traces, flame speed, and flame radius over time.

Figure 3 presents the first parametric analysis, focused on DL instability and p_g. The analysis puts into evidence that increasing p_g leads to faster flame expansion and earlier pressure rise without affecting the ignition process, which is consistent with eq. (15). Moreover, the

FIGURE 2 Effect of a ±50% variation in parameters d_g and E_e on the evolution of flame speed and pressure for hydrogen–air mixtures with 16% H_2 (φ = 0.453, top) and 28% H_2 (φ = 0.926, bottom).

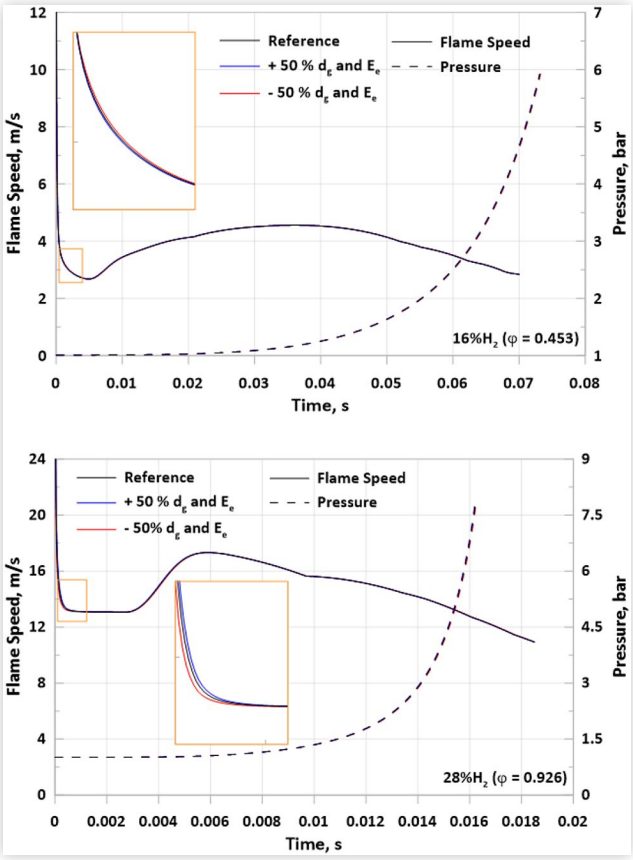

proposed model is much more sensitive to this parameter, indicating that proper selection of p_g is crucial for achieving accurate simulation of unstable combustion processes.

The parametric analysis for TD instability and c_{TD} is shown in Figure 4, which reports a very similar model response to that of Figure 3. In particular, increasing c_{TD} by the same amounts as before causes quite similar faster flame expansions and earlier pressure rises, the only difference being a lower model sensitivity near the end of the combustion process. Again, this indicates that also proper selection of c_{TD} is crucial for accurate simulation of an unstable combustion.

To close the present analysis, it is worth emphasizing that p_g and c_{TD} are considered tuning constants in this work, and their values are selected to find the best agreement with the measurements. At the same time, the value selected for p_g (p_g = 0.6) is fully in line with literature indications [24], while a c_{TD} slightly lower than unity (c_{TD} = 0.9) indicates that the TD-related flame speed enhancement is only marginally lower than that predicted by Howarth. In other words, the values assigned to these constants largely agree with the observations made by other researchers, supporting the physical basis of the proposed approach.

FIGURE 3 Effect of a p_g variation on the evolution of pressure (top), flame speed, and flame radius (bottom) for a mixture with 16% H_2 (φ = 0.453).

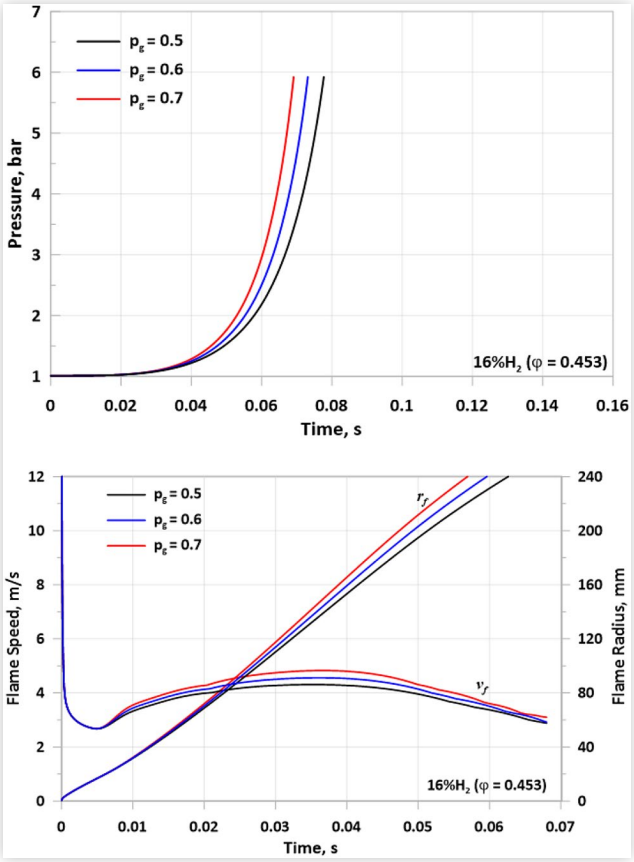

FIGURE 4 Effect of a c_{TD} variation on the evolution of pressure (top), flame speed, and flame radius (bottom) for a mixture with 16% H_2 (φ = 0.453).

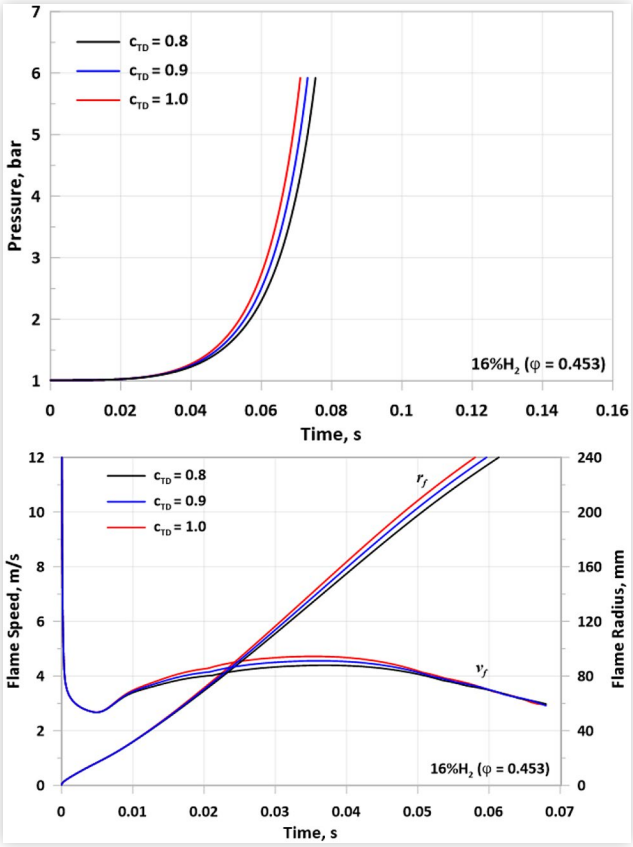

Model Validation and Discussion of Results

In this section a comparison between the experimental results of Goulier et al. [28,29] and the predictions of the proposed ignition-combustion model is presented, investigating first the two leaner test cases (16% and 20% H_2) and then the two closer to stoichiometric conditions (24% and 28% H_2). The experimental data consist of combustion bomb pressure traces, which cover the entire combustion events, and flame radii and expansion speeds, available instead only up to a radius of 80 mm. This lower cap is related to the limitations of the optical Schlieren setup used in the experiments.

Preliminarily, it is interesting to discuss the evolution of the unburned and burned temperatures, shown in Figure 5, together with the trend of correction term ω_f. The figure refers to the two lowest H_2 volume fractions and shows that the flame radius corresponding to the switch between the kernel expansion model and the two-zone model (ω_f < 1.1) tends to reduce as the H_2 volume fraction increases. The kernel formation phase, characterized by a super-adiabatic kernel temperature, is much more relevant at small equivalence ratios: this is because *Le* is furthest away from unity, leading to high positive

FIGURE 5 Evolution of adiabatic flame temperature (purple lines), burned and unburned zone temperatures (red and blue lines), and correction term ω_f (black lines). Solid lines represent the case with 16% hydrogen by volume, while dashed lines refer to 20% hydrogen by volume.

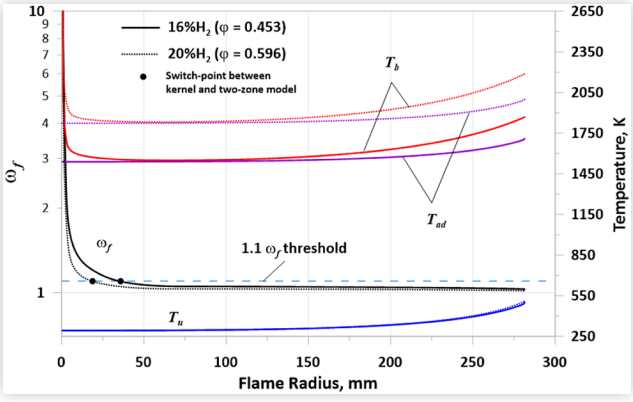

stretch, and S_L^0 is smallest, which magnifies the beneficial role of the initial energy. The figure also highlights that during the terminal phase of the combustion process the burned zone temperature diverges again from the constant-pressure adiabatic temperature, because of the pressure build-up inside the combustion bomb. Despite

FIGURE 6 Comparison of experimental pressure trace (light blue dots) with numerical results for cases with 16% and 20% hydrogen by volume. The red line includes both DL and TD instabilities; the blue line includes only DL instability; the black line represents the case without any instabilities.

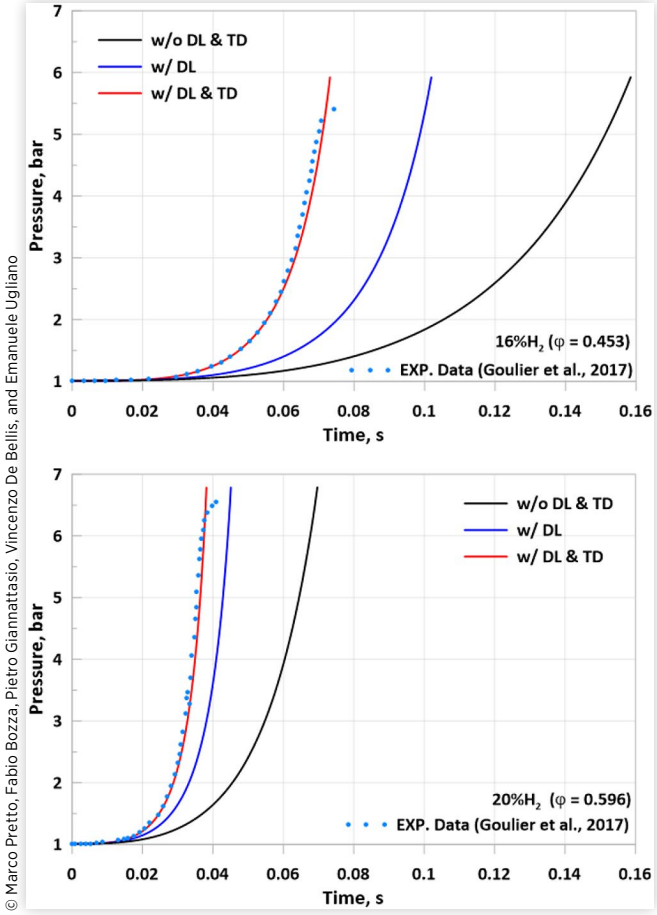

FIGURE 7 Comparison of experimental flame speed and flame radius (light blue dots) with numerical results for cases with 16% and 20% hydrogen by volume. The red line includes both DL and TD instabilities; the blue line includes only the DL instability; the black line represents the case without any instabilities.

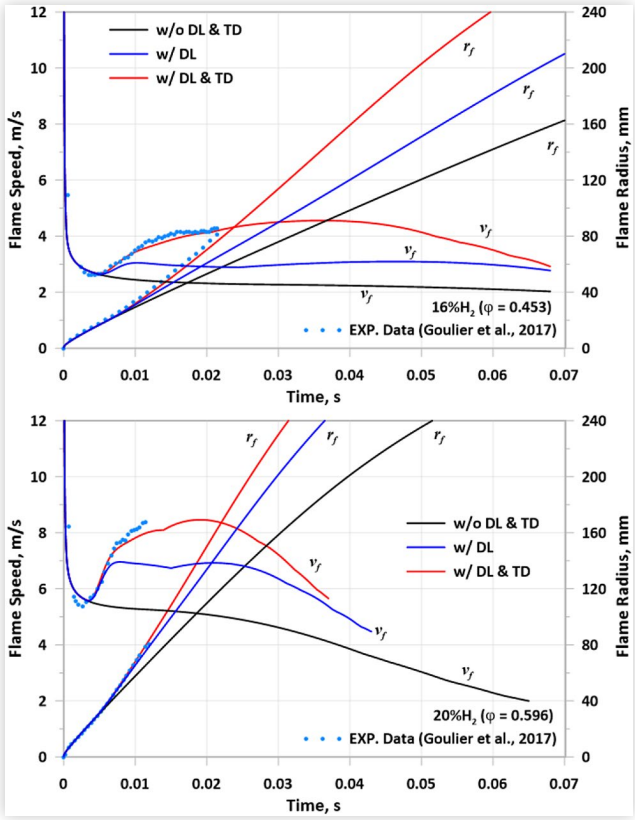

that, any increase in ω_f is inhibited, since it is associated with the stretch rate, $2v_f/r_f$, which tends asymptotically to zero as the kernel grows larger.

The corresponding evolution over time of the pressure traces is reported in Figure 6. The theoretical framework predicts the presence of both hydrodynamic and thermo-diffusive instabilities under the present mixture conditions. Focusing first on the 16% hydrogen case, an excellent agreement is observed between the experimental data (light blue dots) and the simulation (red line) when both flame instability effects are accounted for in the model. Minor discrepancies at the end of the combustion process only depend on the flame-wall interaction, which has been neglected in the model. To evaluate the role of each instability term, two additional simulations were conducted: one excluding all instabilities (black line), and the other including only DL instabilities (blue line). Comparing these traces with the experimental data reveals a significantly slower pressure rise when one or both instabilities are ignored, with the largest deviation occurring in the absence of both. These results highlight the need for incorporating both DL and TD mechanisms to reproduce accurately the experimental pressure trace. Similar conclusions are drawn for the 20% hydrogen case. Here, consistently with the higher Lewis number, the TD instability plays a minor role, highlighting the ability of the proposed model to capture correctly the changes in flame expansion speed in response to different thermochemical properties of the mixture.

To emphasize further these findings, Figure 7 presents the flame speed and flame radius trends for the same hydrogen volume fractions. Focusing on the 16% hydrogen case, the experimental flame speed initially decreases, and then, after reaching a minimum, it increases presumably due to the onset of the flame instabilities. These experimental trends are captured well by the numerical model when both instability effects are included (red line), resulting in an excellent agreement between experimental and predicted time histories of the flame radius. Coherently with the pressure trace analysis, considering only the DL effects leads to predicting a considerably smaller flame speed increase compared to the experimental one, and this deviation is even more pronounced in the absence of both instabilities. Consequently, both scenarios show poor agreement with the experimental flame speed and radius data. Similar conclusions are

FIGURE 8 Flame speed enhancement factors due to hydrodynamic (red lines) and thermo-diffusive (blue lines) instabilities as a function of the flame radius. The solid lines represent the case with 16% hydrogen by volume, while the dashed lines refer to 20% hydrogen by volume.

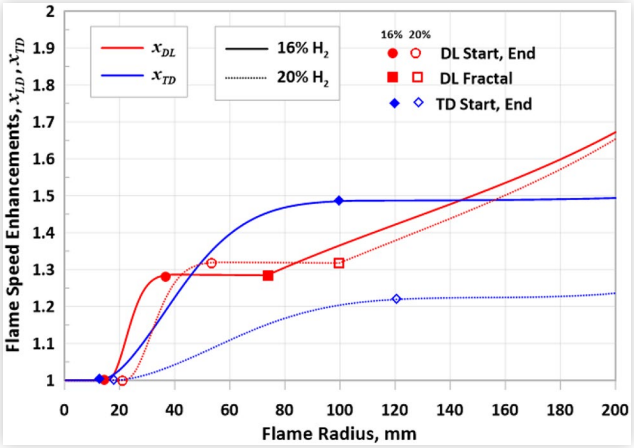

drawn for the 20% hydrogen case, which confirms the model sensitivity to the changes in hydrogen fraction.

The results presented in the previous figures are strongly dependent on the variations over time of enhancement factors x_{DL} and x_{TD}, reported in Figure 8 as a function of the flame radius. The figure hosts two sets of plots that refer to the mixtures with 16% (solid lines) and 20% (dashed lines) hydrogen content by volume. The evolution of x_{DL}, which depends mainly on the density jump across the flame, is quite similar in the two cases. Only minor differences arise in the r_f values that denote the onset and the achievement of a developed DL instability (DL Start and End), with noticeable similarities also between the two fractal-like evolutions (DL Fractal) described by eq. (16). However, the onset of the fractal DL instability results in a small x_{DL} cusp, which can be noticed also in the v_f plots of the 20% H_2 case reported in Figure 7. On the contrary, the TD instabilities are strongly affected by the equivalence ratio, which in turn is related to the Lewis number. As a result, the factor x_{TD} at 20% H_2 (dashed blue line) is substantially lower than that at 16% H_2 (solid blue line). Additionally, in both cases x_{TD} exhibits a slower transition compared to that of x_{DL}, whichever the hydrogen concentration is.

The second part of the discussion focuses on the cases with 24% and 28% hydrogen concentration, as presented in Figure 9. For these two cases, the Lewis number is high enough to suppress completely the TD instabilities. Nevertheless, a strong agreement between experimental and numerical results is still obtained in terms of both flame speed and flame radius. This emphasizes the important role of the ubiquitous DL instability and the reliability of the sub-model used here to quantify its effect, although minor v_f cusps remain as the fractal DL instability takes effect abruptly. The figure also reports the evolution of the burned-relative expansion speed, S_b, defined in eq. (12). It does not account for flame

FIGURE 9 Comparison of experimental flame radii and speeds (light blue scatter plots) with respective numerical results (solid and dotted red lines) for cases with 24% and 28% hydrogen by volume.

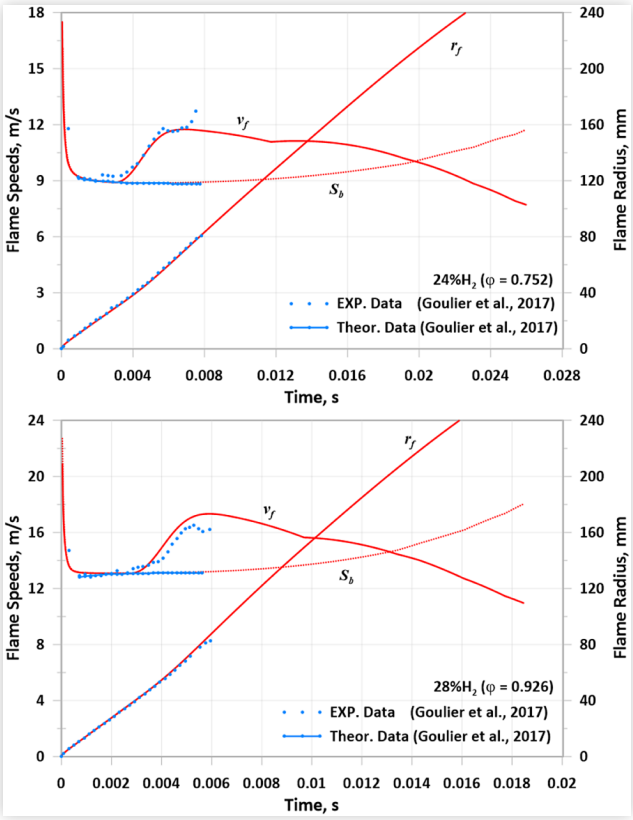

instabilities and can be compared with the corresponding theoretical evolution reported by Goulier, and denoted there as $V_{s,smooth}$ [20]. A close match is achieved once again.

In summary, despite the complexity of the involved thermo-physical phenomena, the predictions of the present integrated model reproduce quite well the available experimental data across all test cases, which is a positive outcome also considering the quasi-0D modeling framework adopted. The overall approach, including the kernel formation and early expansion stage, only required a minimal tuning of the DL and TD intensities (constants p_g and c_{TD}, respectively), which, moreover, were kept fixed across all four cases analyzed. This demonstrates the robustness of the proposed approach in capturing the influence of hydrogen concentration, also in light of the complex flame instability dynamics at play.

Conclusions

This work has presented the development of a predictive model for the estimation of the expansion velocity of laminar hydrogen/air premixed flames in an enclosed volume. The simulation outcomes have been validated against literature experimental data collected for a combustion bomb operated with different hydrogen

volume fractions. To replicate the experimental data, a 0D two-zone combustion model has been integrated with a 1D kernel formation sub-model that describes the early stage of combustion. The effects of hydrodynamic (DL) and thermo-diffusive (TD) instabilities have also been accounted for, in conjunction with their respective onset conditions. The simulation framework demonstrates good predictive capabilities in all tested conditions, without the need for case-by-case tuning, and the proposed integrated ignition-combustion model replicates accurately the experimental pressure traces, as well as the evolution of flame radii and speeds over time. This satisfying outcome highlights the importance of including flame instability mechanisms and their interaction in the combustion model. Indeed, the assumption of purely laminar and smooth flame front leads to excessively long times for the combustion completion compared to the experiments. Moreover, the analysis of the simulation results shows that DL instabilities occurred in all tested conditions, while TD instabilities played a significant role only in the two leaner cases, in which the hydrogen volume fractions of 16% and 20% lead to low mixture Lewis numbers ($Le < 0.6$).

Future developments aim to include in the framework of this integrated model the effects of turbulence on the flame structure, focusing on their likely interaction with the two flame instability mechanisms considered in this work.

References

1. European Commission, "REPowerEU," https://energy.ec.europa.eu/topics/eus-energy-system/hydrogen_en.
2. Novella, R., Gomez-Soriano, J., González-Domínguez, D., and Olaciregui, O., "Understanding the Role of Thermo-Diffusive Instabilities in Hydrogen Combustion for Lean-Burn Spark-Ignition Engine Operation," *Energy Convers Manag* 334 (2025): 119801, doi:10.1016/j.enconman.2025.119801.
3. Kyjovský, Š., Vávra, J., Bortel, I., and Toman, R., "Drive Cycle Simulation of Light Duty Mild Hybrid Vehicles Powered by Hydrogen Engine," *Int J Hydrogen Energy* 48, no. 44 (2023): 16885-16896, doi:10.1016/j.ijhydene.2023.01.137.
4. Darrieus, G., "Propagation D'un Front de Flamme," *La Technique Moderne* 30, no. 18 (1938).
5. Landau, L., "On the Theory of Slow Combustion," in: , *Dynamics of Curved Fronts*, (Elsevier, 1988), 403-411, doi:10.1016/B978-0-08-092523-3.50044-7.
6. Kadowaki, S., "The Effects of Heat Loss on the Burning Velocity of Cellular Premixed Flames Generated by Hydrodynamic and Diffusive-Thermal Instabilities," *Combust Flame* 143, no. 3 (2005): 174-182, doi:10.1016/j.combustflame.2005.05.012.
7. Matalon, M., "The Darrieus–Landau Instability of Premixed Flames," *Fluid Dyn Res* 50, no. 5 (2018): 051412, doi:10.1088/1873-7005/aab510.
8. Denet, B. and Haldenwang, P., "A Numerical Study of Premixed Flames Darrieus-Landau Instability," *Combustion Science and Technology,* 104 (1–3): 143–167, 1995, doi:10.1080/00102209508907714.
9. Pelce, P. and Clavin, P., "Influence of Hydrodynamics and Diffusion Upon the Stability Limits of Laminar Premixed Flames," *J Fluid Mech* 124, no. 1 (1982): 219, doi:10.1017/S002211208200247X.
10. Yu, R., Bai, X.S., and Bychkov, V., "Fractal Flame Structure Due to the Hydrodynamic Darrieus-Landau Instability," *Phys Rev E Stat Nonlin Soft Matter Phys* 92, no. 6 (2015), doi:10.1103/PhysRevE.92.063028.
11. Kwon, C., Hassan, M.I., and Faeth, G.M., "Flame/Stretch Interactions of Heavy-Hydrocarbon/o/n Premixed Flames," *In 37th Aerospace Sciences Meeting and Exhibit* (1999), doi:10.2514/6.1999-321.
12. Wen, X., Zirwes, T., Scholtissek, A., Böttler, H. et al., "Flame Structure Analysis and Composition Space Modeling of Thermodiffusively Unstable Premixed Hydrogen Flames — Part I: Atmospheric Pressure," *Combust Flame* 238 (2022), doi:10.1016/j.combustflame.2021.111815.
13. Wen, X., Zirwes, T., Scholtissek, A., Böttler, H. et al., "Flame Structure Analysis and Composition Space Modeling of Thermodiffusively Unstable Premixed Hydrogen Flames — Part II: Elevated Pressure," *Combust Flame* 238 (2022), doi:10.1016/j.combustflame.2021.111808.
14. Onorati, A., Payri, R., Vaglieco, B.M., Agarwal, A.K. et al., "The Role of Hydrogen for Future Internal Combustion Engines," *International Journal of Engine Research* 23, no. 4 (2022): 529-540, doi:10.1177/14680874221081947.
15. Meziat Ramirez, F.A., Douasbin, Q., Dounia, O., Vermorel, O. et al., "Flame-Turbulence Interactions in Lean Hydrogen Flames: Implications for Turbulent Flame Speed and Fractal Modelling," *Combust Flame* 273 (2025), doi:10.1016/j.combustflame.2024.113926.
16. Kelley, A.P., Jomaas, G., and Law, C.K., "Critical Radius for Sustained Propagation of Spark-Ignited Spherical Flames," *Combust Flame* 156, no. 5 (2009): 1006-1013, doi:10.1016/j.combustflame.2008.12.005.
17. Herweg, R. and Maly, R.R., "A Fundamental Model for Flame Kernel Formation in S. I. Engines," *SAE International* 101 (1992).
18. Ko, Y., Arpaci, V.S., and Anderson, R.W., "Spark Ignition of Propane-Air Mixtures Near the Minimum Ignition Energy: Part II. A Model Development," *Combust Flame* 83, no. 1–2 (1991): 88-105, doi:10.1016/0010-2180(91)90205-P.
19. Pretto, M., Giannattasio, P., De Betta, E., and Bozza, F., "A Consistent Model of the Initiation, Early Expansion, and Possible Extinction of a Spark-Ignited Flame Kernel," *International Journal of Engine Research* 26, no. 2 (2025): 161-175, doi:10.1177/14680874241272812.
20. Pretto, M., De Betta, E., and Giannattasio, P., "Estimating the Minimum Ignition Energy of Spark-Ignited Fuel/Air Mixtures: Preliminary Steps Towards a Novel Modelling Approach," *J Phys Conf Ser* 2893, no. 1 (2024): 012093, doi:10.1088/1742-6596/2893/1/012093.

21. Pretto, M., Giannattasio, P., Grahn, V., Hlaing, P. et al., "Experimental Investigation of the Early Development of Spark-Ignited CH4-Air and C3H8-Air Flame Kernels," *Fuel* 394 (2025): 135110, doi:10.1016/j.fuel.2025.135110.
22. Zaytsev, M. and Bychkov, V., "Effect of the Darrieus-Landau Instability on Turbulent Flame Velocity," *Phys Rev E* 66, no. 2 (2002): 026310, doi:10.1103/PhysRevE.66.026310.
23. Chaudhuri, S., Akkerman, V., and Law, C.K., "Spectral Formulation of Turbulent Flame Speed with Consideration of Hydrodynamic Instability," *Phys Rev E* 84, no. 2 (2011): 026322, doi:10.1103/PhysRevE.84.026322.
24. Bychkov, V.V. and Liberman, M.A., "Dynamics and Stability of Premixed Flames," *Phys Rep* 325 (2000): 115-237, doi:10.1016/S0370-1573(99)00081-2.
25. Berger, L., Attili, A., and Pitsch, H., "Intrinsic Instabilities in Premixed Hydrogen Flames: Parametric Variation of Pressure, Equivalence Ratio, and Temperature. Part 2 – Non-Linear Regime and Flame Speed Enhancement," *Combust Flame* 240 (2022): 111936, doi:10.1016/j.combustflame.2021.111936.
26. Howarth, T.L., Hunt, E.F., and Aspden, A.J., "Thermodiffusively-Unstable Lean Premixed Hydrogen Flames: Phenomenology, Empirical Modelling, and Thermal Leading Points," *Combust Flame* 253 (2023), doi:10.1016/j.combustflame.2023.112811.
27. Howarth, T.L. and Aspden, A.J., "An Empirical Characteristic Scaling Model for Freely-Propagating Lean Premixed Hydrogen Flames," *Combust Flame* 237 (2022): 111805, doi:10.1016/j.combustflame.2021.111805.
28. Goulier, J., Comandini, A., Halter, F., and Chaumeix, N., "Experimental Study on Turbulent Expanding Flames of Lean Hydrogen/Air Mixtures," *Proceedings of the Combustion Institute* 36, no. 2 (2017): 2823-2832, doi:10.1016/j.proci.2016.06.074.
29. Goulier, J., Chaumeix, N., Halter, F., Meynet, N. et al., "Experimental Study of Laminar and Turbulent Flame Speed of a Spherical Flame in a Fan-Stirred Closed Vessel for Hydrogen Safety Application," *Nuclear Engineering and Design* 312 (2017): 214-227, doi:10.1016/j.nucengdes.2016.07.007.
30. Meyer, G. and Wimmer, A., "A Thermodynamic Model for the Plasma Kernel Volume and Temperature Resulting from Spark Discharge at High Pressures," *J Therm Anal Calorim* 133, no. 2 (2018): 1195-1205, doi:10.1007/s10973-018-7169-z.
31. Yu, D. and Chen, Z., "Theoretical Analysis on the Transient Ignition of a Premixed Expanding Flame in a Quiescent Mixture," *J Fluid Mech* 924 (2021): A22, doi:10.1017/jfm.2021.633.
32. Mcbride, B.J., Gordon, S., and Cleveland, A., "NASA Reference Computer Program for Calculation of Complex Chemical Equilibrium Compositions and Applications II. Users Manual and Program Description," : 1311.
33. Zhang, Y., Fu, J., Xie, M., and Liu, J., "Improvement of H2/O2 Chemical Kinetic Mechanism for High Pressure Combustion," *Int J Hydrogen Energy* 46, no. 7 (2021): 5799-5811, doi:10.1016/j.ijhydene.2020.11.083.
34. Beeckmann, J., Hesse, R., Kruse, S., Berens, A. et al., "Propagation Speed and Stability of Spherically Expanding Hydrogen/Air Flames: Experimental Study and Asymptotics," *Proceedings of the Combustion Institute* 36, no. 1 (2017): 1531-1538, doi:10.1016/j.proci.2016.06.194.
35. Jomaas, G., Law, C.K., and Bechtold, J.K., "On Transition to Cellularity in Expanding Spherical Flames," *J Fluid Mech* 583 (2007): 1-26, doi:10.1017/S0022112007005885.

Contact Information

First author: **Marco Pretto,**
University of Udine - Polytechnic Department of Engineering and Architecture, Via delle Scienze 206 33100, Udine, Italy,
at marco.pretto@uniud.it

Corresponding author: **Emanuele Ugliano,**
University of Naples "Federico II", Industrial Engineering Department, Via Claudio 21, 80125, Naples, Italy,
at emanuele.ugliano@unina.it

Acknowledgments

The financial support of the DPIA of the University of Udine under the strategic program "PSD-ESPERT" is gratefully acknowledged.

Definitions/Abbreviations

CEA - Chemical Equilibrium Applications
DL - Darrieus-Landau
TD - Thermo-Diffusive

SYMBOLS

A - Area or deficient reactant
c - Adjustment coefficient
c_p - Isobaric specific heat capacity
d_g - Electrode gap distance
D - Fractal excess
e - Specific internal energy
E - Electrical energy
h - Specific enthalpy
l - Flame thickness
k - Thermal conductivity
Le - Lewis number
$m, \dot{m}$ - Mass, mass flow rate
p - Pressure
p_g - Geometrical parameter for DL instability
Q - Heat of combustion
Q_w - Wall heat transfer
r - Radius

R - Non-dimensional kernel radius
S - Flame speed
T - Temperature
t - Time
U - Non-dimensional expansion speed
V - Volume
v - Expansion velocity
x - Flame speed enhancement
y - Normalized mass fraction
Y - Mass fraction
γ - Ratio of specific heats
η - Energy deposition efficiency
θ - Non-dimensional temperature
Θ - Density ratio
ϑ - Jacobi theta function
$\prod$ - Critical pressure
ρ - Density
τ - Non-dimensional time
φ - Equivalence ratio
ω_f - Non-dimensional reaction rate
ω_2 - Growth rate of the TD perturbations

SUBSCRIPTS

a - Activation
A - Deficient reactant
ad - Adiabatic
b - Burned
bd - Breakdown
c - Critical
cyl - Cylindrical
DL - Darrieus-Landau
e - Electrical
en - Entrainment
f - Flame
i - Initial condition
L - Laminar
TD - Thermo-Diffusive
u - Unburned

ISSN 0148-7191